doi:10.1016/j.jmb.2007.07.041 J. Mol. Biol. (2007) 373, 141–152

JMB

Available online at www.sciencedirect.com
ScienceDirect

ELSEVIER

Structure and Function of the Engineered Multicopper Oxidase CueO from *Escherichia coli*—Deletion of the Methionine-Rich Helical Region Covering the Substrate-Binding Site

Kunishige Kataoka[1], Hirofumi Komori[2], Yusaku Ueki[1], Yusuke Konno[1], Yuji Kamitaka[3], Shinji Kurose[1,3], Seiya Tsujimura[3], Yoshiki Higuchi[2], Kenji Kano[3], Daisuke Seo[1] and Takeshi Sakurai[1]*

[1]*Division of Material Sciences, Graduate School of Natural Science and Technology, Kanazawa University, Kakuma, Kanazawa 920-1192, Japan*

[2]*Graduate School of Life Science, University of Hyogo, 3-2-1 Kouto, Kamigori-cho, Ako-gun, Hyogo 678-1297, Japan*

[3]*Division of Applied Life Sciences, Graduate School of Agriculture, Kyoto University, Kitashirakawa Oiwake-cho, Sakyo-ku, Kyoto 606-8502, Japan*

Received 15 May 2007; received in revised form 16 July 2007; accepted 17 July 2007
Available online 2 August 2007

Edited by R. Huber

CueO is a multicopper oxidase (MCO) that is involved in the homeostasis of Cu in *Escherichia coli* and is the sole cuprous oxidase to have ever been found. Differing from other MCOs, the substrate-binding site of CueO is deeply buried under a methionine-rich helical region including α-helices 5, 6, and 7 that interfere with the access of organic substrates. We deleted the region Pro357–His406 and replaced it with a Gly-Gly linker. The crystal structures of a truncated mutant in the presence and in the absence of excess Cu(II) indicated that the scaffold of the CueO molecule and metal-binding sites were reserved in comparison with those of CueO. In addition, the high thermostability of the protein molecule and its spectroscopic and magnetic properties due to four Cu centers were also conserved after truncation. As for functions, the cuprous oxidase activity of the mutant was reduced to ca 10% that of recombinant CueO owing to the decrease in the affinity of the labile Cu site for Cu(I) ions, although activities for laccase substrates such as 2,2′-azino-bis(3-ethylbenzothiazoline-6-sulfonic acid), *p*-phenylenediamine, and 2,6-dimethoxyphenol increased due to changes in the access of these organic substrates to the type I Cu site. The present engineering of CueO indicates that the methionine-rich α-helices function as a barrier to the access of bulky organic substrates, which provides CueO with specificity as a cuprous oxidase.

Keywords: CueO; multicopper oxidase; homeostasis; truncated mutant; X-ray crystal structure

Introduction

Multicopper oxidases (MCOs) are enzymes containing a multiple copper center that catalyze the oxidation of a variety of substrates, such as polyphenols, aromatic polyamines, L-ascorbate, and metal ions, concomitantly with the four-electron reduction of dioxygen to water.[1–5] Laccase, the largest subfamily of MCOs, shows multiple functions, including lignin degradation, pigmentation, and pathogenesis in fungi, as well as lignin biosynthesis and wound healing in plants.[6–10] Therefore, the structures and functions of new MCOs such as

*Corresponding author. E-mail address: ts0513@kenroku.kanazawa-u.ac.jp.

Abbreviations used: MCO, multicopper oxidase; ABTS, 2,2′-azino-bis(3-ethylbenzothiazoline-6-sulfonic acid); *p*-PD, *p*-phenylenediamine; 2,6-DMP, 2,6-dimethoxyphenol; rCu, regulatory Cu; rCueO, recombinant CueO; PCR, polymerase chain reaction; CD, circular dichroism; DPPH, 1,1-diphenyl-2-picrylhydrazyl; NHE, normal hydrogen electrode; EPR, electron paramagnetic resonance; SUR, structurally unconserved region.

Escherichia coli CueO (formerly called yacK)[11–13] and *Bacillus subtilis* CotA[14,15] have been discussed in comparison with those of laccase.

CueO is a 53.4-kDa periplasmic protein involved in the Cu efflux system, together with CopA, the P-type ATPase.[16] CueO is responsible for the oxidation of cuprous ion to the less toxic cupric ion and for the oxidation of a catechol siderophore, enterobactin.[17,18] CueO also catalyzes the oxidation of organic compounds, including 2,2′-azino-bis(3-ethylbenzothiazoline-6-sulfonic acid) (ABTS), *p*-phenylenediamine (*p*-PD), and 2,6-dimethoxyphenol (2,6-DMP). The oxidase activities of CueO toward these substrates are considerably low but are fairly enhanced in the presence of excess Cu(II) ions.[11,12] That is, the enzymatic activity of CueO is regulated by Cu ions in *E. coli*.

The crystal structures of 11 MCOs—ascorbate oxidase,[19] ceruloplasmin,[20] five fungal laccases,[21–26] Fet3p,[27] CueO,[28] CotA,[29] and phenoxazinone synthase[30]—have been determined. The archetypal MCO consists of about 500 amino acid residues and has three domains, each of which basically has an eight-stranded Greek key β-barrel fold (cupredoxin fold).[31] Cupredoxins are a family of small blue copper (type I Cu) proteins ($M_r \approx 14{,}000$) characterized by a very intense Cys(S$^-$)→Cu(II) charge transfer transition band in the visible spectrum ($\lambda_{max} \approx 600$ nm; $\varepsilon \approx 5000$), high redox potential (+180–680 mV), and narrow hyperfine splitting in the electron paramagnetic resonance (EPR) spectrum ($A_Z \approx 4\times10^{-3}$ to 8×10^{-3} cm^{-1}).[32] Only the C-terminal cupredoxin domain (domain 3) of MCO has a type I Cu site, which transfers electrons from the substrate to the trinuclear Cu center composed of a type II Cu and a pair of type III Cu atoms located at the interface of domains 1 and 3 and reduces dioxygen to two water molecules.

According to the structures of MCOs,[19–27,29,30] the type I Cu site is positioned at the bottom of the widely opened substrate-binding cleft, and an imidazole edge of the type I Cu ligand is exposed to solvent water, whereas the type I Cu site consisting of His443, Cys500, His505, and Met510 in CueO is completely isolated from solvent water by a methionine-rich insertion sequence (amino acid residues 355–400, of which 14 residues are Met) including α-helices 5, 6, and 7. In particular, the longest, helix 5 (amino acid residues 356–371), which includes seven methionine residues, interferes with the access of organic substrates to the type I Cu site (Fig. 1). Beneath helix 5, the labile regulatory Cu (rCu)-binding site comprising Met355, Asp360 (present in helix 5), Asp439, and Met441 is located only 7.5 Å apart from the type I Cu site. Both Cu sites are connected with a hydrogen bond between OD2 of Asp439 and NE2 of His443.[33] The rCu site is the site that binds the substrate Cu(I) ion, although crystal structure analysis of Cu(II)-soaked CueO revealed that a Cu(II) ion was bound at this site. The activities of CueO toward organic substrates are enhanced in the presence of excess Cu(II) because rCu functions as the mediator of electron transfer between substrates and type I Cu.[33]

Several different types of recombinant CueO (rCueO) have been expressed to date, such as Strep-tag-attached rCueO using the vector pASK-IBA3 (IBA) and rCueO without an attached peptide using a specifically controlled expression vector.[11,12] We constructed a new expression system of CueO with 6xHis tag at the C-terminus suitable for purification with immobilized metal ion affinity chromatography. The native CueO, which might be induced by excess Cu supplemented in a culture medium, can be excluded by performing immobi-

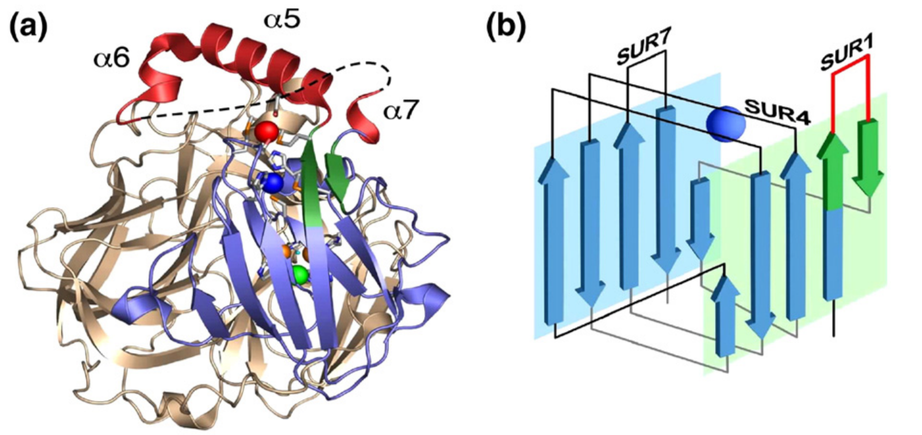

Fig. 1. The structure of CueO and the folding topology of domain 3. (a) Ribbon diagram of CueO. The domain 3 of CueO is shown in blue and red (the antiparallel connections of the first and second β-strands of domain 3 are highlighted in green). The region between α-helix 5 and α-helix 6 (broken line) is not seen because of high mobility. To generate the Δα5–7 deletion mutant, the amino acid residues in the α-helical region from Pro357 to His406 (red) were deleted and replaced by the dipeptide Gly-Gly. Red, blue, green, and orange spheres indicate the labile (regulatory) Cu (rCu), type I Cu, type II Cu, and type III Cu ions, respectively. The figure was drawn with PyMOL[50] using the coordinates from Protein Data Bank file 1N68. (b) Schematic diagram of the β-barrel structure of domain 3. The domain made up of two five-stranded β-sheets (one additional strand is inserted in each sheet) forms the β-sandwich structure. SURs are illustrated by wire. The color scheme is the same as in (a).

lized metal ion affinity chromatography. By using this expression system, we preliminarily prepared a variant of CueO (Δα5–7 CueO) in which 50 amino acid residues (Pro357–His406, of which 13 residues are Met), including α-helices 5, 6, and 7 (red in Fig. 1), and 23 residues spanning between helices 6 and 7 as an unstructured loop (amino acid residues 380–402) were deleted from rCueO, and a Gly-Gly linker to connect antiparallel β-strands was inserted so as not to deform the CueO scaffold.[34] In the present report, we determined the crystal structure of Δα5–7 CueO and studied how the function of this first extensively engineered MCO was modified without changing the scaffold structure and spectroscopic properties.

Results

Structure of Δα5–7 CueO

The crystal structure of Δα5–7 CueO has been determined at 1.81 Å resolution. The asymmetric unit contains two Δα5–7 CueO molecules (molecules A and B), which are related by a pseudo-2-fold symmetry (Supplementary Fig. 1). Both molecules form a head-to-head interaction at the surface region exposed by the deletion of α-helices 5–7, although Δα5–7 CueO is monomeric in solution as evidenced by gel-filtration chromatography (not shown). There is a nitrate ion that probably originated from the crystallization precipitant at the interface between molecules A and B. The overall fold of both molecules is almost identical with that of rCueO[28,33] (the root mean square distance for 435 C^{α} atoms of the molecule A of Δα5–7 CueO with rCueO is 0.39 Å.), except for the loop region between domains 2 and 3 (>2 Å) (Fig. 2 and Supplementary Fig. 2). Figure 3 shows the overall structure of Δα5–7 CueO (molecule A) comprising three domains as rCueO and other MCOs.[19–30] Molecules A and B have essentially the same fold, although the C-terminal 6xHis-tag region of molecule B is disordered (Supplementary Fig. 3). The structural discrepancy at this region between Δα5–7 CueO and rCueO may be caused by crystal packing interaction.

The structures of active sites (Fig. 4, Table 1) are also almost identical with those of rCueO,[28,33] except for the bridging group between type III Cu atoms. In the present Δα5–7 CueO, an oxygen atom has been satisfactorily refined as a bridging species with an acceptable temperature factor at the trinuclear Cu center. On the other hand, a Cl^- ion bridged between type III Cu atoms in rCueO,[28,33] although the OH^--bridged form of rCueO has been reported very recently.[35] The angle around oxygen, Cu2 (type III)–O–Cu3 (type III), in molecule A (molecule B) in the structure of Δα5–7 CueO is 149.8° (146.9°), while that around Cl^-, Cu2 (type III)–Cl–Cu3 (type III), in the structure of rCueO has been reported as 169.3°. Bridging of the naturally occurring group (OH^- or O^{2-}) afforded a bond angle similar to values reported for other MCOs.[19–30] The bonding distances of Cu (type III)–O in molecule A (molecule B) were refined to 1.96 Å (1.96 Å) for Cu2 and to 1.97 Å (1.95 Å) for Cu3, respectively, while those of Cu (type III)–Cl were 2.29 Å (Cu2) and 2.43 Å (Cu3). In addition, the distance of Cu (type II)–O (H_2O or OH^-) has been also reduced from 2.96 Å in rCueO to 2.49 Å (2.52 Å) for molecule A (molecule B) in Δα5–7 CueO, although it is not clear whether the discrepancy was induced directly by deprotonation from the coordinated water molecule or indirectly by the difference in the bridging species between type III Cu atoms. The oxidation state of all Cu atoms is divalent as evidenced by spectroscopies (*vide infra*). The overlapped structures around the fifth copper (rCu)-binding site of rCueO and Δα5–7 CueO (Fig. 4, Roberts, S. A. *et al.* (2002)[28] (Protein Data Bank accession code 1KV7), and Li, X. *et al.* (2007)[35] (2FQF)) indicate that the spatial arrangement of the side chains of Asp439 and Met441 changes upon the binding of a Cu(II) ion at this site.

The crystal structure of Δα5–7 CueO soaked with 10 mM Cu(II) for several seconds has been

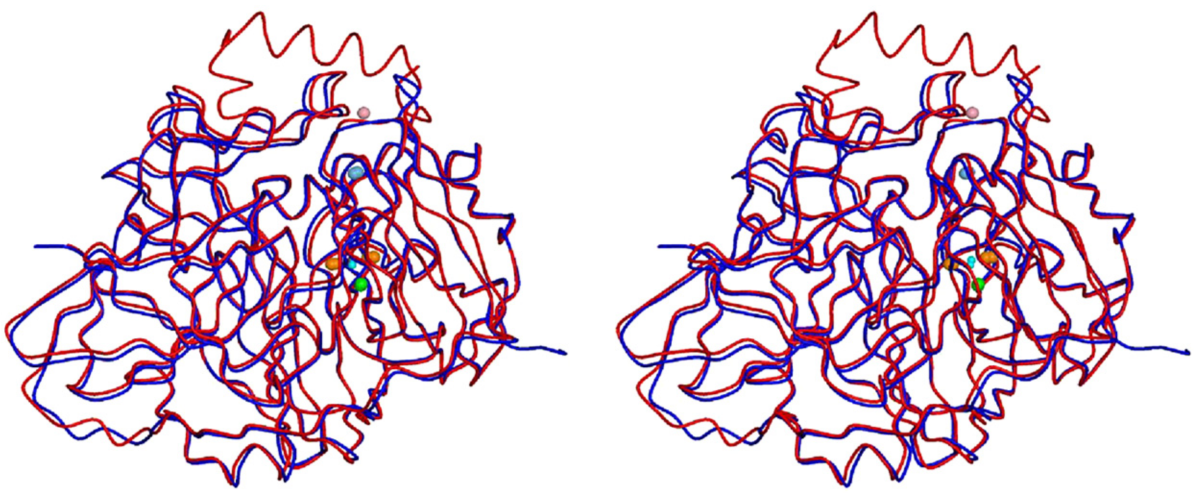

Fig. 2. Superposition of the C^{α} atoms of Δα5–7 CueO (blue) and rCueO (red).

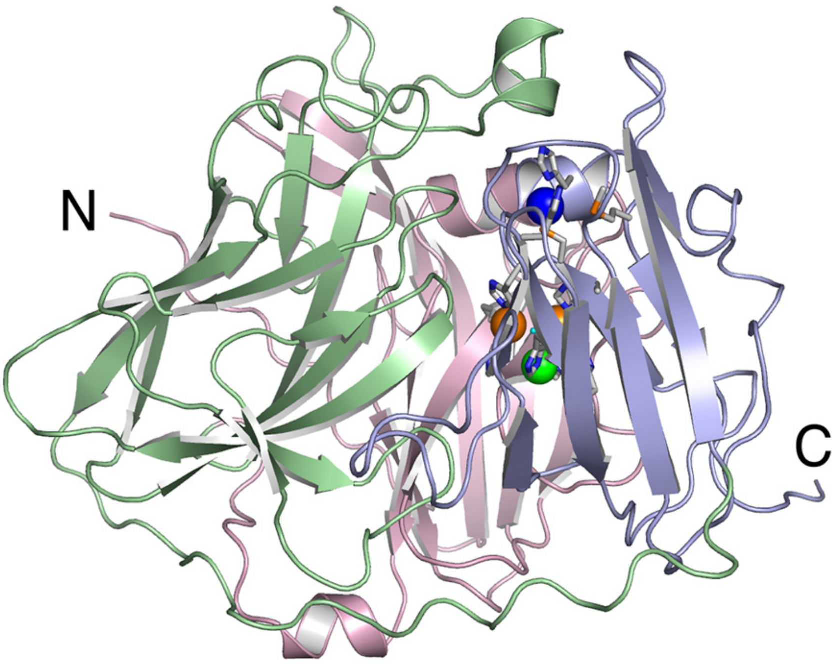

Fig. 3. Overall structure of Δα5–7 CueO (molecule A). Domain 1, pale pink; domain 2, pale green; domain 3, pale blue. Type I Cu, type II Cu, and type III Cu ions are depicted as blue, green, and orange spheres, respectively.

determined at 1.50 Å (Supplementary Figs. 2 and 3b). The soaking of Cu(II) in the crystal of Δα5–7 CueO did not affect the overall folding of the protein molecule, except for the conformational changes around the C-terminal 6xHis-tag region caused by the coordination of exogenous Cu ions. The anomalous difference map of Cu-soaked Δα5–7 CueO showed clear density peaks corresponding to two exogenous Cu ions positioned at the interface of molecules A and B. One Cu is coordinated by His518 (molecule A), His518 (molecule B), and His520 (molecule B), and the other one is coordinated by Glu110 (molecule A), His494 (molecule A), His519 (molecule B), and His522 (molecule B). As mentioned above, the C-terminal region of molecule B is disordered in the structure of Δα5–7 CueO without additional Cu ions. On the contrary, this region of molecule A is disordered in Cu-soaked Δα5–7 CueO. No electron density, which can be assigned as Cu, was found at the rCu-binding site in the structure of Δα5–7 CueO even with excess Cu.

The region at the interface of CueO was flattened after truncation. Although the presence of a deep substrate-binding pocket is not recognized, it is

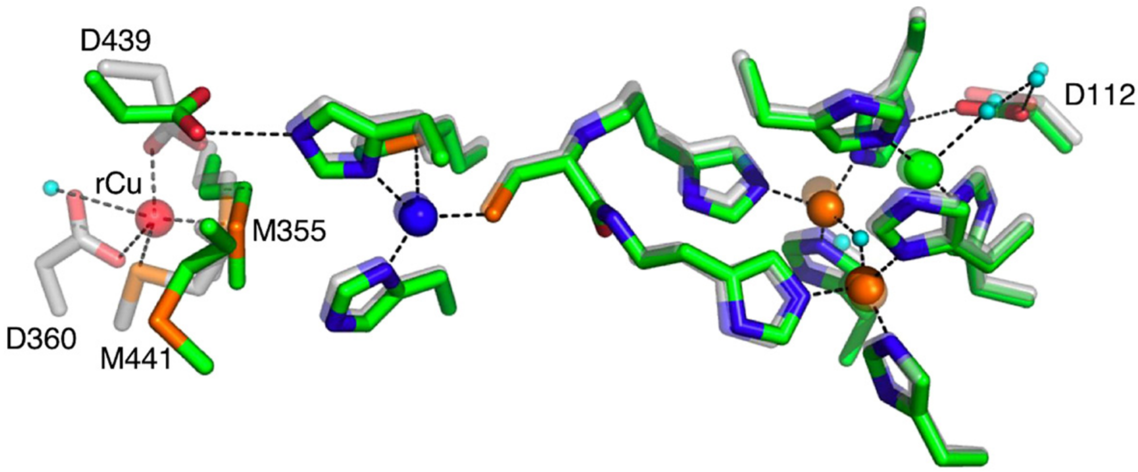

Fig. 4. Superposition of the Cu-binding sites of Δα5–7 CueO onto those of rCueO. Δα5–7 CueO is shown by atomic color coding (green), and rCueO is shown by pale atomic coding. Type I Cu, type II Cu, type III Cu, and rCu are shown as blue, green, orange, and red spheres, respectively. Met355, Asp439, and Met441 are rCu ligands, and Asp360 is deleted in Δα5–7 CueO. Asp112 is the putative proton donor. Type I Cu is ligated by His443, Cys500, His505, and Met510. Type II Cu is ligated by His101, His446, and a water molecule. One type III Cu ion is ligated by His103, His141, and His501, and the other type III Cu ion is ligated by His143, His448, and His 499. An OH^- ion (oxygen atom figures as a small pale-blue sphere) bridges between type III Cu ions.

Table 1. Copper–ligand distances and angles

	Δα5–7 CueO		rCueO
	Molecule A	Molecule B	(1KV7)[28]
Type I Cu			
Cu(1)–His443 (Å)	2.04	2.01	2.02
Cu(1)–Cys500 (Å)	2.15	2.20	2.19
Cu(1)–His505 (Å)	1.99	1.99	1.98
Cu(1)–Met510 (Å)	3.28	3.38	3.23
Type II Cu			
Cu(4)–His101 (Å)	1.98	1.99	1.92
Cu(4)–His446 (Å)	1.96	1.93	1.83
Cu(4)–HOH (Å)	2.49	2.52	2.96
Type III Cu			
Cu(2)–O (Å)	1.97	1.95	2.29
Cu(2)–His143 (Å)	2.02	2.05	2.02
Cu(2)–His448 (Å)	2.03	2.07	1.94
Cu(2)–His499 (Å)	2.04	2.05	2.02
Cu(3)–O (Å)	1.96	1.96	2.43
Cu(3)–His141 (Å)	2.10	2.05	1.97
Cu(3)–His103 (Å)	2.13	2.04	1.96
Cu(3)–His501 (Å)	2.02	2.04	2.09
Cu(2)–Cu(3) (Å)	3.79	3.75	4.70
Cu(2)–Cu(4) (Å)	3.48	3.47	3.54
Cu(3)–Cu(4) (Å)	3.89	3.87	3.98
Cu(2)–O–Cu(3) angle (°)	149.8	146.9	169.3

expected that Δα5–7 CueO will show increased activities for organic substrates by removing the bulky region (*vide infra*). Since the rCu site without Asp360 is now exposed to solvent, it is also expected that its role as the mediator of electron transfer in the presence of excess Cu(II) will be modified.

Spectroscopic and electrochemical properties of Δα5–7 CueO

The electronic absorption spectrum of Δα5–7 CueO, together with that of rCueO, is illustrated in Fig. 5a. A truncated mutant showed intense blue color due to the charge transfer S_π^-(Cys)→Cu(II) originating from type I Cu at 612 nm (ε ≈ 6000 at pH 6.0) similarly to rCueO. The shoulder at about 330 nm (ε ≈ 5000 at pH 6.0) due to the charge transfer OH^-→Cu(II) (type III) was also observed for both rCueO and Δα5–7 CueO.

The circular dichroism (CD) spectral features of rCueO and Δα5–7 CueO were also highly similar over wavelengths of 300–800 nm, affording the charge transfer bands OH^-→Cu(II) (type III) at 330 nm (−), N(His)→Cu(II) at 440 nm (−), S_σ^-(Cys)→Cu(II) at ca 520 nm (+, shoulder), S_π^-(Cys)→Cu(II) at 580 nm (+), and d–d at 745 nm (−) (Fig. 5a).

Both signals due to type I and type II Cu ions were observed in the EPR spectrum of Δα5–7 CueO (solid line in Fig. 5b): spin Hamiltonian parameters were $g_{II}=2.24$ and $A_{II}=6.7\times10^{-3}$ cm^{-1} for type I Cu, and $g_{II}=2.24$ and $A_{II}=19.0\times10^{-3}$ cm^{-1} for type II Cu. These spin Hamiltonian parameters were the same as those of the present rCueO (dotted line) and those of rCueO in Grass, G. *et al.* (2004)[18], although those of type II Cu in rCueO have been reported to be $g_{II}=2.26$ and $A_{II}=15.2\times10^{-3}$ cm^{-1} in Kim, C. *et al.* (2001).[11] This discrepancy might originate from the difference in the assignments of the type II Cu signal (an extra Cu might be present in the case of Kim, C. *et al.* (2001)[11]) or from indirect effect due to the bridging of Cl^- between type III Cu ions (*vide infra*). The total amount of EPR-detectable Cu^{2+} was 1.9 per protein molecule, ensuring that type I Cu and type II Cu ions were fully oxidized and that type III Cu ions were antiferromagnetically coupled. All the spectral features above indicate that the electronic structure of Cu-binding sites in Δα5–7 CueO was not affected at all by the truncation of the helical region.

rCueO did not give clear redox waves on cyclic voltammograms, although the $E°'$ value due to type I Cu could be estimated as +0.36 V *versus* normal hydrogen electrode at pH 6.0 by successive measurements using an Au electrode modified with various promoters (Fig. 6; data not shown). In contrast, Δα5–7 CueO gave unequivocal quasireversible electron transfer responses $E°'=+0.37$ V, with a peak-to-peak separation of $\Delta E_p=87$ mV at pH 6.0, indicating that electric communication between the electrode and

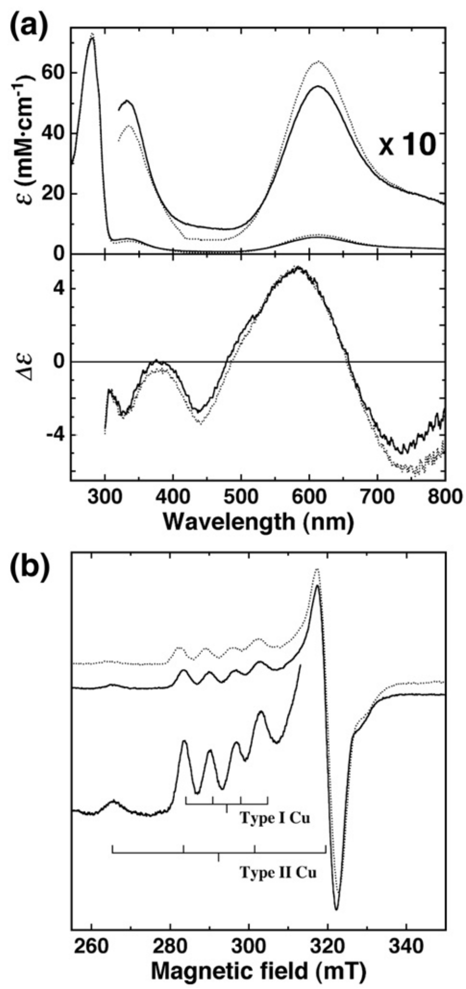

Fig. 5. Electronic absorption (a, top), CD (a, bottom), and EPR spectra (b) of rCueO (dotted line) and Δα5–7 CueO (solid line). Measurement conditions: (a) 0.1 M potassium phosphate buffer (pH 6.0) at room temperature; (b) 0.1 M potassium phosphate buffer (pH 6.0) at 77 K; microwave frequency, 9.20 GHz; microwave power, 5 mW; modulation frequency, 100 kHz; modulation amplitude, 1 mT; filter, 0.1 s; sweep time, 4 min; amplitude, 400.

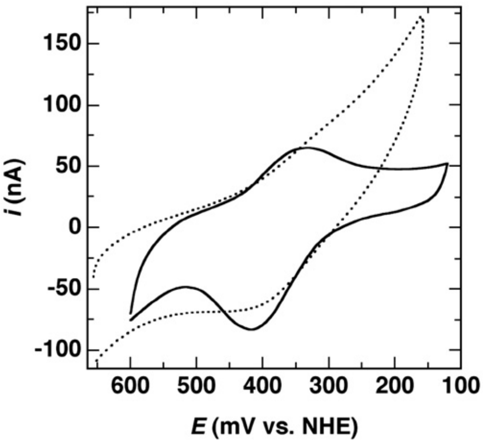

Fig. 6. Cyclic voltammograms of rCueO (dotted line) and Δα5–7 CueO (solid line). The background for Δα5–7 CueO is subtracted. The working electrode is a gold disk modified with thioglycolate. Measurement conditions: 0.1 M potassium phosphate buffer (pH 6.0) at room temperature; protein concentration, 51 μM; scan rate, 2 mV s^{-1}.

the protein molecule became much easier due to truncation without any change in the redox potential of type I Cu (experimental error is ca 0.01 V).

Effect of temperature and pH on the activities and stability of Δα5–7 CueO

Incubations of rCueO and Δα5–7 CueO in 100 mM potassium phosphate buffer, pH 6.0, over the range of 30–75 °C showed that their oxidation activities for *p*-PD increased continuously with increasing temperature; thus, the optimal temperatures of both rCueO and Δα5–7 CueO were found to be higher than 75 °C. As for thermostability, both enzymes retained full activity following incubation at 50 °C for 30 min, whereas about 50% activity was lost by incubation at 60 °C. The half inactivation time of Δα5–7 CueO ($t_{1/2}$=28 min at 60 °C) was slightly shorter than that of rCueO ($t_{1/2}$=38 min) (Supplementary Fig. 4). All these findings indicate that Δα5–7 CueO conserved high thermostability comparable to rCueO in spite of the deletion of 50 amino acids.

The pH dependencies of the oxidase activity of rCueO and Δα5–7 CueO for *p*-PD were determined (pH 2–12). The optimum pH of Δα5–7 CueO was 7.5, slightly lower than that of rCueO (pH 8.0). The stability of Δα5–7 CueO decreased sparingly compared to rCueO over the pH range of 6–11 by incubation at 25 °C for 60 min in the same buffer (data not shown).

Catalytic properties of Δα5–7 CueO

The oxidation of 2,6-DMP by rCueO and Δα5–7 CueO in the presence of various concentrations of Cu(II) ion was studied in order to determine the affinity of the rCu site for Cu(II) (Supplementary Fig. 5). The K_m value of Δα5–7 CueO was determined to be 0.77 mM, five times higher than that of rCueO (K_m=0.14 mM), while V_{max} values were the same (34 U mg^{-1}).

The substrate specificity of Δα5–7 CueO was examined for the oxidation of Cu(I), Fe(II), ABTS, *p*-PD, and some phenolic substrates in comparison with that of rCueO (Table 2). Oxidase activities were measured in the presence and absence of excess Cu(II): 1 mM for rCueO and 10 mM for Δα5–7 CueO. The amount of Cu(II) added was determined based on K_m values to ensure full occupation of the rCu site. The cuprous oxidase activity of Δα5–7 CueO was reduced to ca 10% that of rCueO owing to the decrease in the affinity of the rCu site for Cu(II) ions. The K_m values for Cu(I) were not obtained because inhibition occurred at >0.1 mM Cu(I) and did not reach the saturation condition. The activity of Δα5–7 CueO with Fe(II) was almost the same as that of rCueO.

The truncated mutant demonstrated about 30- and 10-times-higher activities for ABTS and *p*-PD, respectively, contrary to those of rCueO in the absence of exogenous Cu(II), while activities in the presence of excess Cu(II) were comparable to those of rCueO. On the other hand, Δα5–7 CueO exhibited no reactivity with phenolic substrates such as 2,6-DMP, 1,2-benzenediol (catechol), or 2-methoxyphenol (guaiacol) in the absence of Cu(II) ion as in the case of rCueO. However, when excess Cu(II) was present, Δα5–7 CueO showed higher activity with catechol than rCueO. Oxidizing activities with guaiacol and syringaldazine newly emerged in Δα5–7 CueO. Therefore, the effect of the deletion on oxidase activities appears to differ for each substrate depending on the affinity for them.

Table 3 summarizes the steady-state kinetic parameters of rCueO and Δα5–7 CueO for typical laccase substrates ABTS, *p*-PD, and 2,6-DMP. In the

Table 2. Substrate specificities of rCueO and Δα5–7 CueO

	Activity (U mg^{-1})[a]			
	rCueO		Δα5–7 CueO	
Substrate (mM)	Without Cu	1 mM Cu[b]	Without Cu	10 mM Cu[c]
Cu(I) (0.10)[d]	187	201	21	24
Fe(II) (0.5)	0.91	53	0.70	43
ABTS (6.0)	0.45	16	15	34
p-PD (5.0)	0.53	19	4.6	20[e]
2,6-DMP (10.0)	0	29	0	30
Catechol (3.0)	0	12	0	52
Guaiacol (10.0)	0	0	0	5.5
Syringaldazine (0.01)	0	0	0.11	0.29

[a] One unit is the amount of enzyme that oxidizes 1 μmol of substrate per minute in 0.1 M acetate buffer (pH 5.5) at 25 °C.
[b] The activity was measured in the presence of 1 mM $CuSO_4$.
[c] The activity was measured in the presence of 10 mM $CuSO_4$.
[d] The activity was measured with an oxygen electrode, as described in Materials and Methods.
[e] The activity was inhibited by high concentrations of Cu(II) because of complex formation between *p*-PD and Cu(II) and was measured in the presence of 1 mM $CuSO_4$. The activity in the presence of 10 mM $CuSO_4$ was 4.7 U mg^{-1}.

Table 3. Kinetic constants of rCueO and Δα5–7 CueO for ABTS, *p*-PD, and 2,6-DMP in the presence and in the absence of Cu(II) ions

		rCueO		Δα5–7 CueO	
Substrate	Cu(II)[a]	K_m (mM)	V_{max} (U mg^{-1})	K_m (mM)	V_{max} (U mg^{-1})
ABTS	−	6.5±0.3	1.1±0.1	12±1	46±1
	+	6.4±0.3	34±1	11±0.1	39±1
p-PD	−	375±93	55±11	90±9	108±4
	+	ND[b]	ND[b]	ND[b]	ND[b]
2,6-DMP	−	ND[c]	~0	ND[c]	~0
	+	2.5±0.1	48±1	1.8±0.1	35±1

[a] Plus (+) indicates that 1 mM $CuSO_4$ (for rCueO) or 10 mM $CuSO_4$ (for Δα5–7 CueO) was added to the reaction mixture, and minus (−) indicates that $CuSO_4$ was not added.
[b] Not determined due to complex formation between Cu(II) and *p*-PD.
[c] Not determined due to low activity with 2,6-DMP.

oxidation of ABTS by Δα5–7 CueO, the K_m value was double that of rCueO in both the presence and absence of excess Cu(II) (11–12 mM). rCueO exhibited a dramatic increase in the V_{max} values for ABTS (1.1–34 U mg^{-1}) on addition of excess Cu (II). In contrast, Δα5–7 CueO showed V_{max}=46 U mg^{-1} even in the absence of excess Cu(II). The K_m value of Δα5–7 CueO for *p*-PD decreased to 25% that of rCueO, and the V_{max} value increased twofold as a result of helix deletion as well. On the other hand, no significant change in K_m and V_{max} values occurred for the oxidation of 2,6-DMP.

Discussion

The crystal structure of Δα5–7 CueO (Figs. 2 and 3) indicated that the folding of the domain 3 core and interdomain interactions were not disordered by the deletion of the 50 amino acid residues since the β-barrel structure was rigid. The linker dipeptide adequately formed a short reverse turn to connect the antiparallel ends of the β-strands as expected. In the packing of the Δα5–7 CueO molecules, the interface of molecules A and B is mainly formed with the region exposed by the deletion of α-helix 5 from rCueO. The eight conserved segments (β-strands) composing the core structure of each cupredoxin domain of CueO are connected by seven structurally unconserved regions (SURs).[30] The region deleted from CueO (α-helices 5, 6, and 7) and the disordered loop between α-helices 6 and 7 correspond to the variant region of the cupredoxin superfamily (SUR1 in Fig. 1b). Together with SUR4 and SUR7, this region forms the substrate-binding site in MCOs such as ascorbate oxidase[18] and the interface region in a structural variant of MCO family (Cu nitrite reductase) to interact with the redox couple pseudoazurin.[36,37]

The maintenance of the scaffold structure of CueO in the truncated mutant led to the preserved high thermostability (Supplementary Fig. 4). Furthermore, the content of four Cu ions and all spectroscopic features were the same as those of rCueO (Fig. 5) because type I, type II, and type III Cu sites were not modified by the truncation. Therefore, only the initial stage of the reaction of MCO, the access of the substrate to the protein surface, and the following electron transfer to the type I Cu site are affected by the truncation.

Improvement in electrochemical response without any change in the redox potential of type I Cu (Fig. 6) will be derived from the fact that the distance from the protein surface to type I Cu is shortened by about 3–5 Å. The change in the electrostatic potentials of the protein surface before and after the truncation (Supplementary Fig. 6, viewed from the north side) indicates that the area of negative potential decreased, and this might have also led to better electrochemical communication of Δα5–7 CueO with the electrode.

The rCu-binding site comprising Met355, Asp360, Asp439, and Met441 in rCueO is positioned beneath α-helix 5 (above the type I Cu site). Since one of the four ligand residues (Asp360) was involved in the deleted α-helix 5, the binding affinity of the rCu site for Cu(II) was lowered by the truncation (the K_m value changed from 0.14 to 0.77 mM) (Supplementary Fig. 5), and Cu(II) was not bound at the rCu site after the soaking of 10 mM Cu(II). Instead, two Cu ions were found at the interface of molecules A and B involving 6xHis-tag sequences (Supplementary Fig. 2b). The binding of two Cu ions is considered to take place only in the crystalline form of Δα5–7 CueO containing a 6xHis tag in the C-terminus. These Cu ions cannot affect enzyme activities in the presence of excess Cu(II) (Tables 2 and 3) because the *Cys500Ser* mutant, in which the type I Cu site is vacant but the trinuclear Cu center is still able to react with dioxygen, shows no enzyme activity regardless of the presence of excess Cu(II) (unpublished data).

The dramatic decrease in cuprous oxidase activity from 187 to 21 U mg^{-1} was derived from the truncation of Asp360 (Table 2), leading to a decrease in the affinity for Cu(I), although the exact K_m value could not be determined because of inhibition at high Cu(I) concentrations. In addition, the loss of the cage effect of the region covering the rCu site and the deletion of the 13 Met residues frequently found in metal trafficking systems[38] might have also contributed to the decrease in cuprous oxidase activity. In contrast, the change in ferroxidase activity was not significant (from 0.91 to 0.70 U mg^{-1}), suggesting that the affinity for Fe(II) was not greatly lowered by the truncation or that Fe(II) was not bound at the rCu site. The increases in oxidizing activity with ABTS and *p*-PD (by ca 30 and 10 times, respectively) and the newly emerged activity for syringaldazine indicate that the truncation favored the access of these organic substrates to the region near the type I Cu site, as was also indicated by changes in K_m and V_{max} values (Table 3). Nevertheless, 2,6-DMP, catechol, and guaiacol were still not oxidized by Δα5–7 CueO, suggesting that other factors might also influence the specificities for these organic substrates, such as their low affinities towards the "flattened" surface of the Δα5–7 CueO molecule. Namely, the absence of a clevis to accommodate organic substrates did not lead to increases in the affinities for organic substrates (Table 3).

In the case of laccase, the imidazole edge of one of the His residues coordinating with type I Cu is exposed to solvent water on the wall near the bottom of the substrate-binding pocket, functioning as the effective pathway of electron transfer between substrate and type I Cu.[19,22,29] However, α-helix 4, corresponding to SUR1 in domain 2, isolates this amino acid (His443) from solvent water (Figs. 3 and 4), interfering with its direct interaction with organic substrates.

According to the docking structures of an inducer or a substrate with laccase and CotA, an Asp residue located near the type I Cu site assists the binding of the substrate and the abstraction of a proton from it.[22,29] The corresponding amino acid residue in CueO is Asp439, one of the ligands to rCu. The crystal structure of Δα5–7 CueO unequivocally indicates that the carboxy group in the side chain of this amino acid is exposed to solvent after the truncation, although it is still hydrogen-bonded with His443 for type I Cu (Fig. 4). Thus, it appears that Asp439 does not function in the binding of phenolic substrates such as 2,6-DMP and catechol and/or in deprotonation from them (Table 2).

All modifications in enzyme activities as above are in the absence of excess Cu(II) ion. The extent of the decrease in the cuprous oxidase activity of Δα5–7 CueO was practically the same regardless of the presence of rCu (Table 2) because Cu(II) formed as the product possibly functioned as the mediator of electron transfer between Cu(I) in bulk water and type I Cu.[11,12] The increase in the ferroxidase activities of rCueO and Δα5–7 CueO in the presence of rCu was also derived from the function of rCu as the mediator of electron transfer between the substrate and type I Cu. The oxidizing activities of Δα5–7 CueO for ABTS and *p*-PD, which increased ca 10–30 times even in the absence of rCu, increased further in the presence of rCu (Table 2). Analogous K_m values for the oxidation of ABTS by both rCueO and Δα5–7 CueO, regardless of the presence and absence of excess Cu (Table 3), indicate that the access of ABTS to the protein molecule may not involve the rCu site. (Soaking of ABTS did not give the docked structure.) On the other hand, the emergence of the 2,6-DMP and catechol oxidase activities of both rCueO and Δα5–7 CueO in the presence of rCu (Table 2) might be due to this Cu as the mediator of electron transfer. Increases in the redox potential of type I Cu in the CotA mutant *Met502Leu/Phe*[15] and the decrease in the redox potential of type I Cu in the bilirubin oxidase mutant *Met467Gln*[4] led to decreases in enzyme activities, but the redox potential of type I Cu did not change with the present deletion (Fig. 6). Therefore, the increase or the emergence of the oxidizing activities of Δα5–7 CueO with catechol, guaiacol, and syringaldazine in the presence of rCu might be accounted for by the fact that these organic substances interacted with the region including the rCu site.

These kinetic results evidenced that the deletion of the 50 amino acid residues facilitated the access of organic substrates to the exposed rCu site directly or to the type I Cu site indirectly. Therefore, we can conclude that the presence of the unique region covering the rCu site represents the molecular architecture of CueO needed to produce the specificity for Cu(I). The facile electron transfer between the electrode and the type I Cu site in Δα5–7 CueO (Fig. 6) also supports that the truncated region functions as a barrier to organic substrates. The catalytic efficiency (V_{max}/K_m) for *p*-PD at pH 7.5 was remarkably increased by the truncation from 0.15 to 1.2 U mg^{-1} mM^{-1}, a value comparable to that for bilirubin oxidase (8.5 U mg^{-1} mM^{-1} at pH 6.5)[39] and for laccase from *Lentinula edodes* (2.8 U mg^{-1} mM^{-1} at pH 5.0).[40] Δα5–7 CueO is the first example of the successful modification of MCO function to a large extent, and extensive engineering of the protein molecule is expected to lead to the creation of novel functions.

Materials and Methods

Materials

The vector pUC18 (Takara Biochemicals) was used for DNA cloning and recombinant protein expression. *E. coli* JM109 was used for gene manipulations, and *E. coli* BL21 (Novagen) was used for protein expression. *Taq* DNA polymerase, restriction endonucleases, and other modifying enzymes were obtained from Takara Biochemicals and TOYOBO. Oligonucleotides were purchased from BEX (Japan). All other chemicals were of analytical grade.

Protein expression and purification of rCueO

The 1.6-kb gene fragment consisting of the structural gene of CueO (*yacK*), 6xHis tag, EcoRI linker, and BamHI linker was amplified by polymerase chain reaction (PCR) using *E. coli* JM109 genomic DNA as the template and two oligonucleotides (P1, 5′-GAAGAATTCATGCAACGTCGTGATTTCTTAAAAT-3′ coding for the N-terminal region of CueO and the EcoRI digestion sequence (underlined); P2, 5′-TTGGATCCTTAATGATGATGATGATGATGGCCTACCGTAAACCCTAAC-3′ coding for the 6xHis tag attached to the C-terminal region of CueO, termination codon, and BamHI digestion sequence (underlined)). PCR products were digested with EcoRI and BamHI and cloned into pUC18 digested with EcoRI and BamHI to yield pUCCueO. The inserted gene was analyzed by DNA sequencing.

E. coli BL21 cells containing pUCCueO were grown in liquid LB medium supplemented with 1 mM $CuCl_2$, 0.5 mM IPTG, and 0.1 mg ml^{-1} sodium ampicillin for 12 h at 32 °C, with shaking. Periplasmic fractions of the cells were obtained by cold osmotic shock as follows. *E. coli* cells used to express rCueO were harvested by centrifugation (10,000*g* for 10 min) and washed with cold 10 mM Tris–HCl buffer, pH 8.0 (the same volume as the culture medium). The washed cells were suspended in a 20%

sucrose solution buffered at pH 8.0 with 100 mM Tris–HCl (25% volume of the medium) and left on ice for 10 min. After centrifugation, the cells were resuspended with ice-cold water (20% volume of the medium) containing Complete protease inhibitor cocktail (Roche). The cell suspension was further left on ice for 10 min and then centrifuged at 10,000*g* for 20 min. The supernatant was centrifuged again (90,000*g* for 30 min) to obtain a crude periplasmic fraction.

The periplasmic fraction was applied directly to a BD TALON cobalt affinity resin (BD Biosciences) column equilibrated with 50 mM potassium phosphate buffer (pH 7.0) containing 300 mM NaCl. After washing the column with the same buffer, rCueO was eluted with the same buffer supplemented with 150 mM imidazole. The recombinant protein was further purified using an UnoQ-12 column (Bio-Rad) equilibrated with 20 mM Tris–HCl (pH 8.0). The recombinant protein was eluted with a linear gradient of NaCl (0–1.0 M) in the same buffer. Protein purity was confirmed by SDS-PAGE.

The total Cu content in rCueO was 3.6 per protein molecule, as determined by atomic absorption spectroscopy (the experimental error in determining the Cu content was ca 10%), indicating that four intrinsic Cu ions were incorporated into the active site. The Cu content did not increase after the action of Cu(II) under air or the action of Cu(I) under Ar and dialysis against the buffer solution, ensuring that apoprotein was not present.

Protein engineering of Δα5–7 CueO

To delete 50 residues (Pro357–His406), including α-helices 5, 6, and 7 and the loop between helices 6 and 7, mutagenesis was performed with a two-step PCR method[41,42] using pUCCueO as the template and using sense and antisense mutagenic oligonucleotides designed to lack amino acid codons from Pro357 to His406 but to insert codons for Gly-Gly (underlined) as a linker to connect between Asp356 and Ala407 (P3, 5′-GTTGGCACCACCGTCCATGGAGAGTTGCAGCTTGCGTAC-3′; P4, 5′-CTCTCCATGGACGGTGGTGCCAACAAAATCAACGGTC-3′). After the second PCR using primers P1 and P2, the amplified fragment was digested with EcoRI and BamHI and cloned into pUC18 to yield pUCCueO Δα5–7. The truncated mutant gene was sequenced and expressed in *E. coli* BL21 to purify the mutant protein. Δα5–7 CueO was isolated similarly to rCueO. The m/z value of Δα5–7 CueO was determined to be 48,725 (the calculated value of apoprotein Δα5–7 CueO is 48,652) using matrix-assisted laser desorption/ionization time-of-flight mass spectroscopy, during which a portion of Cu was lost by ionization, although atomic absorption spectroscopy indicated the presence of 3.7 Cu atoms in a protein molecule.

Crystallization, structure determination, and refinement

Crystallization was performed with the sitting-drop vapor-diffusion method at 20 °C using equal volumes of protein (2 μl) and precipitant (2 μl) solutions consisting of 16% polyethylene glycol 3350, 160 mM potassium nitrate, and 20% glycerol. Crystals appeared after a few days and grew to approximate dimensions of around 0.2×0.2×0.1 mm within 1 week. X-ray diffraction data sets were collected at 100 K with freezing in a nitrogen cold stream. The crystal diffracts to 1.81 Å resolution using a rotating anode source (RIGAKU RA-Micro7). The crystal-to-detector distance was maintained at 120 mm with a 0.5° oscillation range per image, covering a total oscillation range of 180°. Determination of unit-cell parameters and integration of reflections were performed using the program MOSFLM.[43] The space group is P_1, and the unit-cell parameters were determined to be a=49.98 Å, b=50.95 Å, c=86.05 Å, α=83.2°, β=90.8°, and γ=66.7°. The Δα5–7 CueO with exogenous copper ion was prepared by soaking the crystal in a reservoir solution containing 10 mM $CuSO_4$. X-ray diffraction data sets of copper-soaked Δα5–7 CueO were collected at a synchrotron source (beam line BL38B1, SPring-8). Structure was determined by the molecular replacement method with the program MOLREP,[44] using the structure of rCueO as a starting model. Simulated annealing refinement was carried out with CNS (Crystallography & NMR System).[45] Alternate rounds of model building and refinement were carried out for further completion of the model using $2F_o-F_c$ and F_o-F_c maps with the interactive molecular graphics program Coot.[46] The progress of TLS (Translation/Libration/Screw) refinement with REFMAC[47] was assessed by monitoring the R-free value for 5% of the total reflection excluded from minimization.[48] The final model consists of molecules A and B of Δα5–7 CueO, and a nitrate ion from the crystallization buffer binds to their interface, which is produced by the deletion of α-helices 5–7. Data collection and refinement statistics are presented in Table 4. Model geometry was analyzed with the program PROCHECK,[49] and no residues were found in the disallowed region of the Ramachandran plot. The figures were prepared by the programs PyMOL†,[50] MOLSCRIPT,[51] Raster3D,[52] and MolFeat (FiatLux).

Table 4. X-ray crystallographic data

	Data 1	Data 2 (Cu-soaked)	Data 3 (Cu-soaked)
Source	RA-Micro7	SPring BL38B	SPring BL38B
Wavelength (Å)	1.542	1.000	1.378
Space group	P_1	P_1	
Cell constants			
a, b, c (Å)	49.98, 50.95, 86.05	50.33, 51.57, 86.70	
α, β, γ (°)	83.2, 90.8, 66.7	83.8, 90.4, 67.1	
Resolution (Å)	30.0–1.81 (1.90–1.81)	30.0–1.50 (1.55–1.50)	30.0–2.27 (2.37–2.27)
Completeness (%)	92.1 (85.8)	95.2 (94.7)	90.51 (88.6)
Redundancy	2.0	2.0	2.0
$I/\sigma(I)$	14.1 (3.0)	35.0 (6.6)	32.6 (27.5)
R_{merge} (%)	5.5 (31.2)	3.4 (9.7)	3.2 (4.6)
R value (%)	17.2 (17.8)	18.0 (22.3)	
R-free (%)	20.8 (22.3)	20.8 (24.1)	
Number of reflections	65,489 (2118)	1,271,073 (2118)	
Number of protein atoms	6768	6772	
Number of hetero atoms	14	16	
Number of water oxygen atoms	394	658	

Spectral and electrochemical measurements

Absorption spectra were measured on JASCO Ubest-50 and JASCO V-560 spectrometers. CD spectra were measured on a JASCO J-500C spectropolarimeter.

† pymol.sourceforge.net

X-band EPR spectra were recorded on a JEOL JES-RE1X spectrometer at 77 K. The total amount of EPR-detectable Cu^{2+} was determined by the double-integration method using Cu-ethylenediaminetetraacetic acid as standard. Signal intensities due to differences in tuning conditions were calibrated with 1,1-diphenyl-2-picrylhydrazyl as an external standard. The content of Cu per protein molecule was determined on a Varian SpectrAA-50 atomic absorption spectrometer. Cyclic voltammetric measurements were carried out using a Bioanalytical Systems Model CV-50W voltammetric analyzer with a three-electrode system consisting of a Ag/AgCl reference electrode, a platinum plate counterelectrode, and a thioglycolate-modified gold working electrode under an Ar atmosphere at 25 °C.

Kinetic analysis

The oxidase activities of rCueO and Δα5–7 CueO were determined by the absorption increases of oxidized products or by the amount of consumed dioxygen detected using a Clark-type oxygen electrode connected to an Oxygraph 9 DO monitor (Central Kagaku) at 25 °C. The oxidation reactions of ABTS, 2,6-DMP, *p*-PD, $FeSO_4 \cdot (NH_4)_2SO_4 \cdot 6H_2O$ (Mohr's salt), catechol, guaiacol, and syringaldazine were followed by initial absorption changes at 420 nm ($\varepsilon = 36{,}000\ M^{-1}\ cm^{-1}$), 477 nm ($\varepsilon = 14{,}800\ M^{-1}\ cm^{-1}$), 487 nm ($\varepsilon = 14{,}700\ M^{-1}\ cm^{-1}$), 315 nm ($\varepsilon = 2200\ M^{-1}\ cm^{-1}$), 450 nm ($\varepsilon = 2000\ M^{-1}\ cm^{-1}$), 436 nm ($\varepsilon = 6600\ M^{-1}\ cm^{-1}$), and 525 nm ($\varepsilon = 65{,}000\ M^{-1}\ cm^{-1}$), respectively, in 0.1 M acetate buffer (pH 5.5). For the determination of cuprous oxidase activity, $[Cu(I)(MeCN)_4]PF_6$ (Sigma) was used as described by Singh *et al.*[17] Inactivations of rCueO and Δα5–7 CueO were followed for 2 h at 60 °C. Enzyme activities depending on pH were measured in a 100-mM Britton–Robinson buffer.

Protein Data Bank accession codes

Coordinates and structure factors have been deposited in the RCSB Protein Data Bank with accession codes 2YXV (Δα5–7 CueO) and 2YXW (Cu-soaked Δα5–7 CueO).

Acknowledgements

Financial support from the Nagase Science and Technology Foundation (to K. Kataoka), NEDO (New Energy and Industrial Technology Development Organization) (to K. Kano), Toyota Motor Corporation (to K. Kano and T. Sakurai), the Foundation of the University of Hyogo (to H. Komori), the Hyogo-ken Science Foundation (to H. Komori), the Yamanouchi Foundation for Research on Metabolic Disorders (to H. Komori), the Inamori Foundation (to H. Komori), the Japanese Aerospace Exploration Agency Project (to Y. Higuchi), and Grants-in-Aid for Scientific Research from the Ministry of Education, Science, Culture, and Sports, Japan (18770093 to H. Komori, 16074214 and 18GS0207 to Y. Higuchi, and 19350081 to T. Sakurai), and MANDOM Corporation (to T. Sakurai) is greatly acknowledged.

Supplementary Data

Supplementary data associated with this article can be found, in the online version, at doi:10.1016/j.jmb.2007.07.041

References

1. Messerschmidt, A. (ed) (1997). Multi-Copper Oxidases, World Scientific, Singapore.
2. Solomon, E. I., Sundaram, U. M. & Machonkin, T. E. (1996). Multicopper oxidases and oxygenases. *Chem. Rev.* **96**, 2563–2605.
3. Baldrian, P. (2006). Fungal laccases—occurrence and properties. *FEMS Microbiol. Rev.* **30**, 215–242.
4. Kataoka, K., Kitagawa, R., Inoue, M., Naruse, D., Sakurai, T. & Huang, H. W. (2005). Point mutations at the type I Cu ligands, Cys457 and Met467, and at the putative proton donor, Asp105, in *Myrothecium verrucaria* bilirubin oxidase and reactions with dioxygen. *Biochemistry*, **44**, 7004–7012.
5. Quintanar, L., Stoj, C., Wang, T. P., Kosman, D. J. & Solomon, E. I. (2005). Role of aspartate 94 in the decay of the peroxide intermediate in the multicopper oxidase Fet3p. *Biochemistry*, **44**, 6081–6091.
6. Leonowicz, A., Cho, N. S., Luterek, J., Wilkolazka, A., Wojtas-Wasilewska, M., Matuszewska, A. *et al.* (2001). Fungal laccase: properties and activity on lignin. *J. Basic Microbiol.* **41**, 185–227.
7. Bajpai, P. (1999). Application of enzymes in the pulp and paper industry. *Biotechnol. Prog.* **15**, 147–157.
8. Claus, H., Faber, G. & König, H. (2002). Redox-mediated decolorization of synthetic dyes by fungal laccases. *Appl. Microbiol. Biotechnol.* **59**, 672–678.
9. Galante, Y. M. & Formantici, C. (2003). Enzyme applications in detergency and in manufacturing industries. *Curr. Org. Chem.* **7**, 1399–1422.
10. Pointing, S. B. (2001). Feasibility of bioremediation by white-rot fungi. *Appl. Microbiol. Biotechnol.* **57**, 20–33.
11. Kim, C., Lorenz, W. W., Hoopes, J. T. & Dean, J. F. (2001). Oxidation of phenolate siderophores by the multicopper oxidase encoded by the *Escherichia coli yacK* gene. *J. Bacteriol.* **183**, 4866–4875.
12. Grass, G. & Rensing, C. (2001). CueO is a multi-copper oxidase that confers copper tolerance in *Escherichia coli*. *Biochem. Biophys. Res. Commun.* **286**, 902–908.
13. Ueki, Y., Inoue, M., Kurose, S., Kataoka, K. & Sakurai, T. (2006). Mutations at Asp112 adjacent to the trinuclear Cu center in CueO as the proton donor in the four-electron reduction of dioxygen. *FEBS Lett.* **580**, 4069–4072.
14. Martins, L. O., Soares, C. M., Pereira, M. M., Teixeira, M., Costa, T., Jones, G. H. & Henriques, A. O. (2002). Molecular and biochemical characterization of a highly stable bacterial laccase that occurs as a structural component of the *Bacillus subtilis* endospore coat. *J. Biol. Chem.* **277**, 18849–18859.
15. Durão, P., Bento, I., Fernandes, A. T., Melo, E. P., Lindley, P. F. & Martins, L. O. (2006). Perturbations of the T1 copper site in the CotA laccase from *Bacillus subtilis*: structural, biochemical, enzymatic and stability studies. *J. Biol. Inorg. Chem.* **11**, 514–526.
16. Rensing, C. & Grass, G. (2003). *Escherichia coli* mechanisms of copper homeostasis in a changing environment. *FEMS Microbiol. Rev.* **27**, 197–213.

17. Singh, S. K., Grass, G., Rensing, C. & Montfort, W. R. (2004). Cuprous oxidase activity of CueO from *Escherichia coli*. *J. Bacteriol.* **186**, 7815–7817.
18. Grass, G., Thakali, K., Klebba, P. E., Thieme, D., Müller, A., Wildner, G. F. & Rensing, C. (2004). Linkage between catecholate siderophores and the multicopper oxidase CueO in *Escherichia coli*. *J. Bacteriol.* **186**, 5826–5833.
19. Messerschmidt, A., Ladenstein, R., Huber, R., Bolognesi, M., Avigliano, L., Petruzzelli, R. *et al.* (1992). Refined crystal structure of ascorbate oxidase at 1.9 Å resolution. *J. Mol. Biol.* **224**, 179–205.
20. Bento, I., Peixoto, C., Zaitsev, V. N. & Lindley, P. F. (2007). Ceruloplasmin revised: structural and functional roles of various metal cation-binding sites. *Acta Crystallogr. Sect. D*, **63**, 240–248.
21. Ducros, V., Brzozowski, A. M., Wilson, K. S., Ostergaard, P., Schneider, P., Svendson, A. & Davies, G. J. (2001). Structure of the laccase from *Coprinus cinereus* at 1.68 Å resolution: evidence for different 'type 2 Cu-depleted' isoforms. *Acta Crystallogr. Sect. D*, **57**, 333–336.
22. Bertrand, T., Jolivalt, C., Briozzo, P., Caminade, E., Joly, N., Madzak, C. & Mougin, C. (2002). Crystal structure of a four-copper laccase complexed with an arylamine: insights into substrate recognition and correlation with kinetics. *Biochemistry*, **41**, 7325–7333.
23. Piontek, K., Antorini, M. & Choinowski, T. (2002). Crystal structure of a laccase from the fungus *Trametes versicolor* at 1.90-Å resolution containing a full complement of coppers. *J. Biol. Chem.* **277**, 37663–37669.
24. Antorini, M., Herpoël-Gimbert, I., Choinowski, T., Sigoillot, J. C., Asther, M., Winterhalter, K. & Piontek, K. (2002). Purification, crystallisation and X-ray diffraction study of fully functional laccases from two ligninolytic fungi. *Biochim. Biophys. Acta*, **1594**, 109–114.
25. Hakulinen, N., Kiiskinen, L. L., Kruus, K., Saloheimo, M., Paananen, A., Koivula, A. & Rouvinen, J. (2002). Crystal structure of a laccase from *Melanocarpus albomyces* with an intact trinuclear copper site. *Nat. Struct. Biol.* **9**, 601–605.
26. Garavaglia, S., Cambria, M. T., Miglio, M., Ragusa, S., Iacobazzi, V., Palmieri, F. *et al.* (2004). The structure of *Rigidoporus lignosus* laccase containing a full complement of copper ions, reveals an asymmetrical arrangement for the T3 copper pair. *J. Mol. Biol.* **342**, 1519–1531.
27. Taylor, A. B., Stoj, C. S., Ziegler, L., Kosman, D. J. & Hart, P. J. (2005). The copper–iron connection in biology: structure of the metallo-oxidase Fet3p. *Proc. Natl Acad. Sci. USA*, **102**, 15459–15464.
28. Roberts, S. A., Weichsel, A., Grass, G., Thakali, K., Hazzard, J. T., Tollin, G. *et al.* (2002). Crystal structure and electron transfer kinetics of CueO, a multicopper oxidase required for copper homeostasis in *Escherichia coli*. *Proc. Natl Acad. Sci. USA*, **99**, 2766–2771.
29. Enguita, F. J., Martins, L. O., Henriques, A. O. & Carrondo, M. A. (2003). Crystal structure of a bacterial endospore coat component. A laccase with enhanced thermostability properties. *J. Biol. Chem.* **278**, 19416–19425.
30. Smith, A. W., Camara-Artigas, A., Wang, M., Allen, J. P. & Francisco, W. A. (2006). Structure of phenoxazinone synthase from *Streptomyces antibioticus* reveals a new type 2 copper center. *Biochemistry*, **45**, 4378–4387.
31. Murphy, M. E., Lindley, P. F. & Adman, E. T. (1997). Structural comparison of cupredoxin domains: domain recycling to construct proteins with novel functions. *Protein Sci.* **6**, 761–770.
32. Nersissian, A. M. & Shipp, E. L. (2002). Blue copper-binding domains. *Adv. Prot. Chem.* **60**, 271–340.
33. Roberts, S. A., Wildner, G. F., Grass, G., Weichsel, A., Ambrus, A., Rensing, C. & Montfort, W. R. (2003). A labile regulatory copper ion lies near the T1 copper site in the multicopper oxidase CueO. *J. Biol. Chem.* **278**, 31958–31963.
34. Kurose, S., Kataoka, K., Otsuka, K., Tsujino, Y. & Sakurai, T. (2007). Promotion of laccase activities of *Escherichia coli* cuprous oxidase, CueO by deleting the segment covering the substrate binding site. *Chem. Lett.* **36**, 232–233.
35. Li, X., Wei, Z., Zhang, M., Peng, X., Yu, G., Teng, M. & Gong, W. (2007). Crystal structure of *E. coli* at different copper concentrations. *Biochem. Biophys. Res. Commun.* **354**, 2126–2131.
36. Kukimoto, M., Nishiyama, M., Tanokura, M., Adman, E. T. & Horinouchi, S. (1996). Studies on protein–protein interaction between copper-containing nitrite reductase and pseudoazurin from *Alcaligenes faecalis* S-6. *J. Biol. Chem.* **271**, 13680–13683.
37. Kataoka, K., Yamaguchi, K., Kobayashi, M., Mori, T., Bokui, N. & Suzuki, S. (2004). Structure-based engineering of *Alcaligenes xylosoxidans* copper-containing nitrite reductase enhances intermolecular electron transfer reaction with pseudoazurin. *J. Biol. Chem.* **279**, 53374–53378.
38. Banci, L. & Rosata, A. (2003). Structural genomics of proteins involved in copper homeostasis. *Acc. Chem. Res.* **36**, 215–221.
39. Kataoka, K., Tanaka, K., Sakai, Y. & Sakurai, T. (2005). High-level expression of *Myrothecium verrucaria* bilirubin oxidase in *Pichia pasatoris*, and its facile purification and characterization. *Protein Expression Purif.* **41**, 77–83.
40. Nagai, M., Sato, T., Watanabe, H., Saito, K., Kawata, M. & Enei, H. (2002). Purification and characterization of an extracellular laccase from the edible mushroom *Lentinula edodes*, and decolorization of chemically different dues. *Appl. Microbiol. Biotechnol.* **60**, 327–335.
41. Kataoka, K., Furusawa, H., Takagi, K., Yamaguchi, Y. & Suzuki, S. (2000). Functional analysis of conserved aspartate and histidine residues located around the type 2 copper site of copper-containing nitrite reductase. *J. Biochem.* **127**, 345–350.
42. Higuchi, R. (1989). In *PCR Technology: Principles and Applications for DNA Amplification* (Erlich, H. A., ed), pp. 61–88, Stockton Press, New York.
43. Powell, H. R. (1999). The Rossmann Fourier autoindexing algorithm in MOSFLM. *Acta Crystallogr. Sect. D*, **55**, 1690–1695.
44. Vagin, A. & Teplyakov, A. (2000). An approach to multi-copy search in molecular replacement. *Acta Crystallogr. Sect. D*, **56**, 1622–1624.
45. Brunger, A. T., Adams, P. D., Clore, G. M., DeLano, W. L., Gros, P., Grosse-Kunstleve, R. W. *et al.* (1998). Crystallography and NMR system: a new software suite for macromolecular structure determination. *Acta Crystallogr. Sect. D*, **54**, 905–921.
46. Emsley, P. & Cowtan, K. (2004). Coot: model-building tools for molecular graphics. *Acta Crystallogr. Sect. D*, **60**, 2126–2132.
47. Winn, M. D., Isupov, M. N. & Murshudov, G. N. (2001). Use of TLS parameters to model anisotropic

displacements in macromolecular refinement. *Acta Crystallogr. Sect. D*, **57**, 122–133.
48. Brunger, A. T. (1992). The free *R* value: a novel statistical quantity for assessing the accuracy of crystal structures. *Nature*, **355**, 472–474.
49. Morris, A. L., MacArthur, M. W., Hutchinson, E. G. & Thornton, J. M. (1992). Stereochemical quality of protein structure coordinates. *Proteins: Struct. Funct. Genet.* **12**, 345–364.
50. DeLano, W. L. (2002). *The PyMOL Molecular Graphics Systems*, DeLano Scientific, San Carlos, CA, USA. http://www.pymol.org.
51. Kraulis, P. J. (1991). MOLSCRIPT: a program package to produce both detailed and schematic plots of protein structures. *J. Appl. Crystallogr.* **24**, 946–950.
52. Merrit, E. A. & Murphy, M. E. (1994). Raster3D Version 2.0: a program for photorealistic molecular graphics. *Acta Crystallogr. Sect. D*, **50**, 869–873.